Jurnal Teknologi

Full paper

Viscous Flow Computation around the Wigley Hull with the Maneuvering Motion using the Inertial Coordinate System on the Non-inertial Grids

Yan Naing Win[a*], Yasuyuki Toda[a]

[a]*Department of Naval Architecture and Ocean Engineering, Osaka University, Osaka, Japan 565-0871*

*Corresponding author: Yan_Naing_Win@naoe.eng.osaka-u.ac.jp

Article history

Received :27 July 2013
Received in revised form :
5 November 2013
Accepted :25 November 2013

Graphical abstract

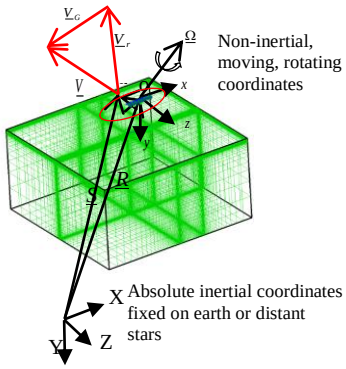

Abstract

Computational Fluid Dynamics (CFD) technique for ship hydrodynamics has been well developed with advanced capabilities for resistance and propulsion, seakeeping, and maneuvering. The Authors' laboratory (Laboratory 3 of Department of Naval Architecture and Ocean Engineering in Osaka University) specializes in resistance and propulsion field and has carried out several simulations based on the CFD code in non-inertial ship-fixed coordinates system. The purpose of this research is to transform the present computation code to the one in inertial coordinate and to investigate the flow field around the Wigley hull for several motions up to three degrees of freedom (3 DOF). The transformed code is simulated on the flat plate initially and the nature of the flow field is investigated and confirmed with the hydrodynamics theory. Then, the wigley hull motions are simulated in several ways such as; uniform motion, pure yaw and circular motion test. The features of the flow field and hydrodynamic forces acting on the hull are discussed based on the computed results. Finally, the propeller effect is implemented behind the wigley hull using the body-force concept by the quasi-steady infinite bladed Blade Element Theory and a propulsion characteristic is observed. The transformed computation code in inertial coordinate is found to be much easier to simulate the different kinds of maneuvering motions compared to the code in non-inertial system and this paper covers the detailed transformation steps and the discussions on the computation results of different motions.

Keywords: Inertial coordinate; flat plate; wigley; uniform flow; pure yaw; circular motion test; body-force; blade element theory

1.0 INTRODUCTION

The advent of computer technology becomes a great tool for ship designing field and Computational Fluid Dynamics (CFD) is one of the branches. CFD method offers an alternative to the traditional build and test design approach, i.e., simulation based design (SBD). As the ship hull form geometry is complex and the fluid flow around the ship is in a very difficult mode to cope with, many approaches might be needed in the design of a ship. It has been conjectured that SBD will offer innovative approaches to design an out-of-box concepts with improved performance.[5]

Consequently, it becomes a must to develop computation code on the other side of experimental works. The purpose of this research, the transformation of the original code into an alternative solution methodology, might be a corner for preceding more steps forward in the research activity of the authors' laboratory. The governing equations, Navier-Stokes Equations in inertial coordinate system, are transformed into the body-fitted grid in the moving coordinate system and the velocity components are defined at earth-fixed coordinate. A single block domain grid is generated around the flat plate and Wigley model. The 12 points Finite Analytic Method (FAM) for space discretization and Euler Implicit Scheme for time discretization are used along with the PISO algorithm for velocity-pressure coupling.[4] The transformed code is simulated with the Wigley hull up to three degrees of freedom by implementing any desired motion of the ship that will be much easier than that of the computation in non-inertial frame.

At the same time, the transformed code in inertial frame is very convenient for the computation of the ship with the propeller effect. In this research, the propeller grid is not used and the propeller effect is computed by the body-force concept with the infinite bladed Blade Element Theory.[8] The computed body-force components are solved in the source terms of the Navier-Stokes equations and the thrust and torque forces are computed within the RANS code.[8] The concept works well in this case and the methodology can be fully applied in other propulsion computations for further research activities.

2.0 METHOD OF COMPUTATION

2.1 Grid Generation

The H-type grid is generated around the zero thickness flat plate as well as the Wigley Hull with the same domain size and number

of grids. The computational domain covers from -1 to +4 in x-direction, from 0 to +3 in y-direction and from -3 to +3 in z-direction. The total grid size is $(91\times41\times51)$ and the Wigley hull geometry is simply developed by Equation 1 with the non-dimensional length 1. The breadth to length ratio used was 0.1 and depth to length ratio was 0.125 which is the standard Wigley Hull. The generated grid domains are shown in Figure 1.

$$z_b = \frac{1}{2}B\left\{1-\left(\frac{2x}{L}\right)^2\right\}\left\{1-\left(\frac{y}{D}\right)^2\right\} \quad (1)$$

L, B and D referred to length, breadth and depth of the hull and z_b is the half breadth. The grid domains are generated by the grid generation code of the Authors' laboratory by setting small meshes near the body surface for capturing of the detailed flow field near the surface. The body part is covered by 41 and 21 grid points in x and y direction respectively. The minimum grid spacing was 0.0015 in non-dimensional lengths in y and z-direction. The grids generation is checked to be more orthogonal by solving the Poisson's equation.

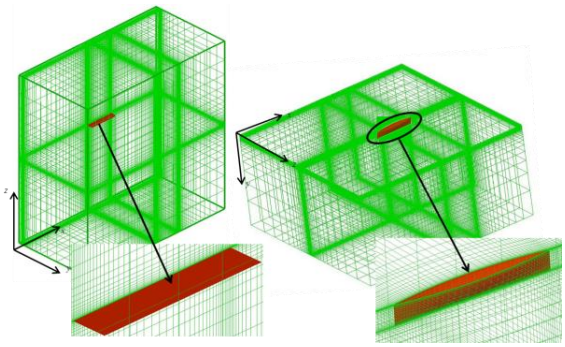

Figure 1 Grids and domain size of flat plate and Wigley model

2.2 Coordinate Transformation

As the purpose of this research is to develop the computation code in inertial frame, the relation between the non-inertial and inertial frames is shown in Figure 2. In non-inertial coordinate (x, y, z) which is fixed on the body (red oval in Figure 2), every single point on its wet surface will have corresponding relative velocity to the surrounding fluid denoted by V_r. Therefore, the momentum equation in this frame is shown in Equation 2 with body force term $\underline{a}_{rel}$ (Equation 3) and the continuity equation is as in Equation 4.

$$\left[\frac{\partial \underline{V}_r}{\partial t'} + \underline{V}_r.\nabla\underline{V}_r\right] = -\rho\underline{a}_{rel} - \nabla(p+\gamma.y) + \frac{1}{Rn}\nabla^2\underline{V}_r \quad (2)$$

$$\underline{a}_{rel} = \ddot{\underline{R}} + 2\underline{\Omega}\times\underline{V}_r + \underline{\Omega}\times(\underline{\Omega}\times\underline{r}) + \dot{\underline{\Omega}}\times\underline{r} \quad (3)$$

$$\nabla.\underline{V}_r = 0 \quad (4)$$

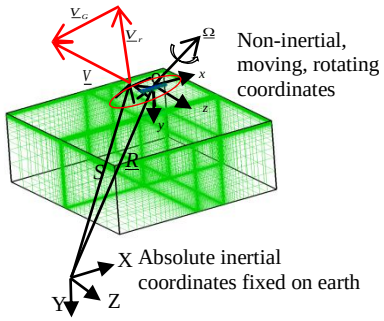

Figure 2 Relation between non-inertial and inertial frames

In inertial coordinate (X, Y, Z), the momentum and continuity equations are written in Equation 5-6 with the grid velocity (Equation 7) in inertial frame which is corresponded to the translating velocity $\dot{\underline{R}}$ and rotational term $\underline{\Omega}\times\underline{r}$. The absolute velocity $\underline{V}$ in inertial frame is the resultant of the relative velocity $\underline{V}_r$ and grid velocity $\underline{V}_G$.

$$\left[\frac{\partial \underline{V}}{\partial t} + (\underline{V}-\underline{V}_G)\nabla\underline{V}\right] = -\nabla(p+\gamma.Y) + \frac{1}{Rn}\nabla^2\underline{V} \quad (5)$$

$$\nabla.\underline{V} = 0 \quad (6)$$

$$\underline{V}_G = \dot{\underline{R}} + \underline{\Omega}\times\underline{r} \quad (7)$$

The governing equation in the new computation code is Equation 5 and it is modified for free movement in 3 DOF of the grid, leaving the velocity components in inertial frame. For the purpose of ease, the transformation is performed in components form. The moving grid position which is a combination of the translational and rotational motion as a function of time are as shown Equation 8-11 where (X_0, Y_0, Z_0) is the arbitrary grid position in inertial frame with the geometry shown in Figure 3 and t' is the time represented in non-inertial frame.

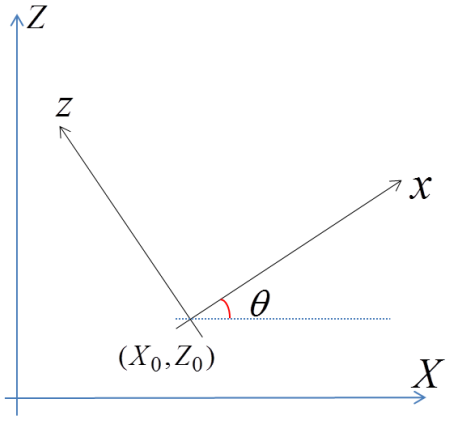

Figure 3 Moving grid geometry

$$X = X_0(t) + x\cos(\theta(t)) - z\sin(\theta(t)) \quad (8)$$

$$Z = Z_0(t) + x\sin(\theta(t)) + z\cos(\theta(t)) \quad (9)$$

$$Y = Y_0(t) = 0 \quad (10)$$

$$t = t' \quad (11)$$

Using these relations, the momentum equation (Equation 5) is operated differentially by each term and then transformed from the physical domain to the computational domain in non-orthogonal curvilinear coordinate $(\xi,\eta,\varsigma,\tau)$. A partial transformation is used in which only the independent variables are transformed, leaving the velocity components in physical domain. But, all the velocities and geometrical coefficients in the transformed equations still belong to the moving coordinate. According to the purpose of this computation, the velocity components (u,v,w) are defined in the absolute inertial earth-fixed coordinates (X,Y,Z) so the velocity components with corresponding geometrical coefficients must be transformed back into inertial coordinates. Finally, the momentum equations with the velocity components in inertial coordinates in the moving non-inertial grids are obtained and written in Equation 12 in general form. The terms u_G, v_G, w_G are the grid velocities in (X,Y,Z) which are dependable on translational and rotational movements as a function of time (Equation 17-19). The corresponding coefficients are shown in Equation 20-24.

$$g^{11}\phi_{\xi\xi} + g^{22}\phi_{\eta\eta} + g^{33}\phi_{\varsigma\varsigma} = A\phi_{\xi} + B\phi_{\eta} + C\phi_{\varsigma} + D\phi_{\tau} + S_{\phi} \quad (12)$$

$$A = \frac{Rn}{J}\left(b_1^1(u-u_G) + b_2^1(v-v_G) + b_3^1(w-w_G)\right) - f^1 \quad (13)$$

$$B = \frac{Rn}{J}\left(b_1^2(u-u_G) + b_2^2(v-v_G) + b_3^2(w-w_G)\right) - f^2 \quad (14)$$

$$C = \frac{Rn}{J}\left(b_1^3(u-u_G) + b_2^3(v-v_G) + b_3^3(w-w_G)\right) - f^3 \quad (15)$$

$$D = R_n \quad (16)$$

$$u_G = \frac{dX_0(t)}{dt} - z\frac{d\theta(t)}{dt}\cos(\theta(t)) - x\frac{d\theta(t)}{dt}\sin(\theta(t)) \quad (17)$$

$$v_G = \frac{dY_0(t)}{dt} = 0 \quad (18)$$

$$w_G = \frac{dZ_0(t)}{dt} + x\frac{d\theta(t)}{dt}\cos(\theta(t)) - z\frac{d\theta(t)}{dt}\sin(\theta(t)) \quad (19)$$

$$b_l^i = \varepsilon_{lmn}\frac{\partial X^m}{\partial \xi^j}\frac{\partial X^n}{\partial \xi^k}(i,j,k-cyclic) \quad (20)$$

$$g^{ij} = \frac{1}{J^2}b_l^i b_l^j \quad (21)$$

$$J = \begin{vmatrix} X_\xi & X_\eta & X_\zeta \\ Y_\xi & Y_\eta & Y_\zeta \\ Z_\xi & Z_\eta & Z_\zeta \end{vmatrix} \quad (22)$$

$$f^i = \frac{1}{J}\frac{\partial}{\partial \xi^j}\left(Jg^{ij}\right) \quad (23)$$

$$S_\phi = \frac{Rn}{J}\left[b_j^1\frac{\partial p}{\partial \xi} + b_j^2\frac{\partial p}{\partial \eta} + b_j^3\frac{\partial p}{\partial \zeta}\right] - 2\left(g^{12}\phi_{\xi\eta} + g^{13}\phi_{\xi\varsigma} + g^{23}\phi_{\eta\varsigma}\right) - f_{b_i} \quad (24)$$

In Equation 24, f_{b_i} is the body force and the body forces will be implemented in this term when the propeller effect is included.

2.3 Computational Outline

The transformed equation (Equation 12) is discretized by the 12-point Finite-Analytic method in space and Euler implicit scheme for time along with the PISO algorithm for velocity-pressure coupling. For one time step, sufficient iterations are repeated to get a time-accurate solution. The finite analytic coefficients are updated for retaining the non-linear nature of the Navier-Stokes equations for each internal-iteration. The laminar flow computation is carried out at R_n = 10,000 with zero Fraud's number (F_n). In the case of the grid domain inclined with some angles, all the geometrical coefficients must need to be calculated, updated and transformed back into inertial frame at each time step and the velocity-pressure field satisfying Navier-Stokes equations and continuity equation is obtained.

$$F_{\text{Pressure}} = -\int_s p n_i dS \quad (25)$$

$$F_{shear} = \int_s \tau_{s_{ij}} n_i dS \quad (26)$$

The hydrodynamics force on the body surface is obtained by integration of the normal and tangential stresses over the wetted surface area. The fluid stress tensor is composed of the components due to pressure and viscous stress. The pressure and shear forces are calculated by Equation 25-26. The combination of the axial component of the forces is the resistance. τ_{sij} is the shear stress component, n_i is the unit-vector normal to the body surface and dS is the local surface area element.

2.4 Boundary Condition

The boundary condition of the computation is shown in Equation 27-30. In the inertial frame, the velocity components and pressure value in the far field could be almost zero. This condition can make the computation much easier to get the converged solution compared to the computation in non-inertial frame.

Inlet : $u = v = w = p = 0$ (27)

Far field : $gradient(u,v,w,p) = 0$ (28)

Free surface (i.e., y=0) : $v = 0$ (29)

On the body surface : $u = u_G, v = v_G, w = w_G$ (30)

■3.0 COMPUTATION IN MANEUVERING MOTIONS

3.1 Computation in Uniform Flow

The flat plate with non-dimensionalized length 1, breadth 0.2 and zero thickness is simulated by the transformed code with the body speed gradually accelerating from 0 to 1 towards the negative X-direction and then keeping at steady state with advanced speed, $u_G = 1$. The computational frictional force of flat plate is checked by the well-known Blasius solution (B/L × 0.01328) and the accelerated condition is checked by the infinite plate theory (Equation 31). Good agreement is observed and shown in Figure 4. Velocity distributions on the Wigley hull is shown in Figure 5.

$$F_{frictional} = (2\times 1.182\times \sqrt{t}\,/\sqrt{Rn}\times\frac{B}{L}) \quad (31)$$

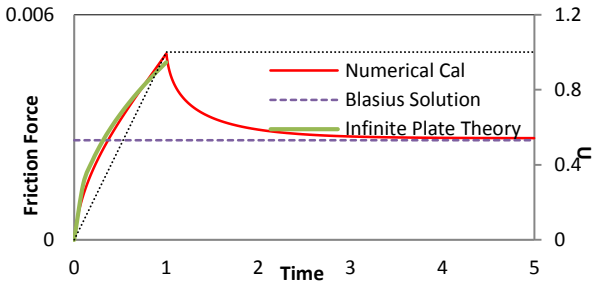

Figure 4 Checking of frictional force on the flat plate

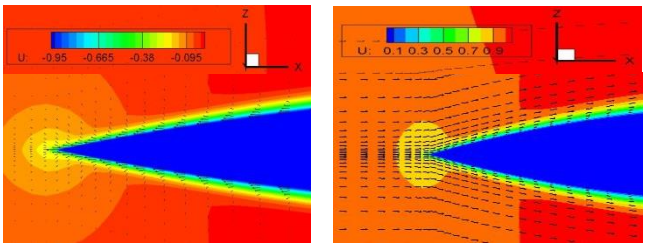

Figure 5 Velocity distributions on the Wigley hull

The pressure force distribution in X-direction is represented by Figure 6. The added mass effect is well observed during the acceleration between t= 0 to 1 and as the steady state approaches, the force becomes constant. The shear force distribution on the hull surface is shown in Figure 7.

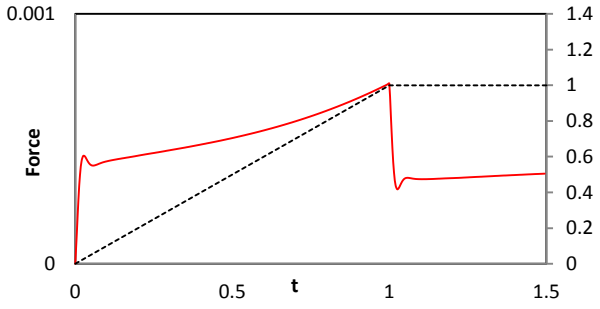

Figure 6 Pressure force distribution on the Wigley hull

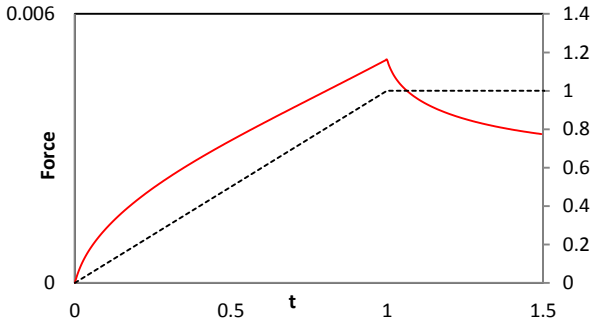

Figure 7 Shear force distribution on the Wigley hull

3.2 Computation in Pure Drift

In nature, the ocean going vessels might probably meet Beam Sea and Oblique Sea that can be a great impact on the hull as well as a disturbance on the maneuvering behavior. After the Wigley hull has been tested in uniform flow, it is then computed with some drift angle to see how the hull surface pressure is distributed.

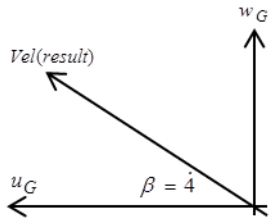

Figure 8 Motion algorithm of pure drift

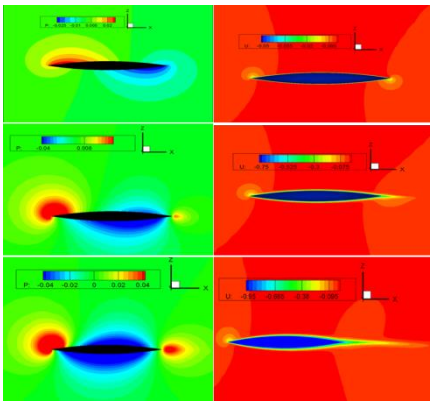

Figure 9 Pressure (left) and velocity (Right) layout in pure drift test.

The ship is given by a motion with drift angle of 4 degree (Figure 8). The resultant velocity is accelerated first and then kept at constant at 1 for the remaining. The grid velocities u_G and w_G can be calculated as in Equation 32 where β is drift angle and implemented into the motion program of the code. The pressure field and the velocity layout along the hull are shown in Figure 9.

$$u_G = Vel(result) * \cos\beta$$
$$w_G = Vel(result) * \sin\beta \quad (32)$$

3.3 Computation in Rotational Motion

When the ship has lateral movement, there might be vorticity generated along the hull and the pressure will be distributed in high difference. In the PMM test like pure yaw, there will be similar phenomenon so that the ship is simply tested rotationally as any movement of the ship can easily be carried out in inertial frame computation code. The ship is fixed at the center point in (x, z) plane at (0.5, 0) and simply given the motion as in Equation 33 with the angular acceleration α with the time t. The vorticity generated along the hull while rotating is investigated by Equation 34 and shown in Figure 10.

$$\theta(t) = \frac{1}{2}\alpha t^2 \tag{33}$$

$$\left.\begin{aligned} \omega_X &= \frac{\partial w}{\partial Y} - \frac{\partial v}{\partial Z} \\ \omega_Y &= \frac{\partial u}{\partial Z} - \frac{\partial w}{\partial X} \\ \omega_Z &= \frac{\partial v}{\partial X} - \frac{\partial u}{\partial Y} \end{aligned}\right\} \tag{34}$$

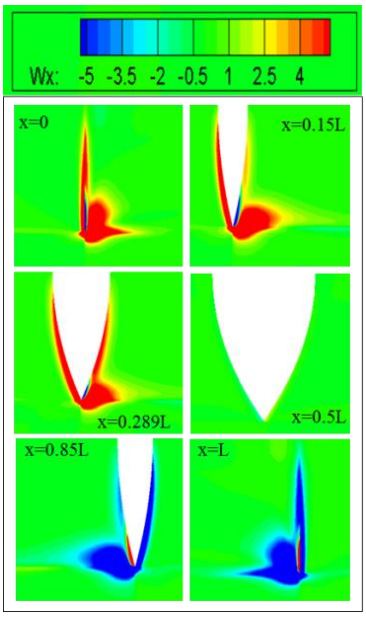

Figure 10 Vorticity distributions along the hull

3.4 Computation in Pure Yaw

In the steady movement with $u_G = 1$, the hull is given the sway velocity w_G. The sway distance is a sinusoidal sine with a function of frequency as shown in Equation 35 where A is the amplitude of the motion, ω is the frequency, t is the time. In this case, amplitude is taken as 0.05; frequency is 2.094 with the period (T) of 3 non-dimensionally. The sway velocity is the differentiation of the sway distance with respect to time and shown in Equation 36. The value of w_G is imposed by zero as there is no movement in y-direction. Additional to sway motion, the yaw angle and the corresponding yaw rate are imposed as in Equation 38 and Equation 39.

$$Z_0(t) = A\sin(\omega t) \tag{35}$$

$$w_G = \dot{Z}_0(t) = A\omega\cos(\omega t) \tag{36}$$

$$\omega = 2\pi / T \tag{37}$$

$$\theta(t) = \tan^{-1}\frac{w_G}{u_G} \approx \frac{w_G}{u_G} = \frac{A\omega\cos(\omega t)}{u_G} \tag{38}$$

$$\dot{\theta}(t) = \frac{\ddot{Z}_0(t)}{u_G} = \frac{-A\omega^2\sin(\omega t)}{u_G} \tag{39}$$

For the yaw rotation, the referenced point is taken at the center of gravity of the plate at $(0.5,0)$ in (x,z) plane. Centered at this point, the ship is rotated in a sinusoidal cosine with a function of frequency (Equation 38). The sway and yaw movements are ninety-degree phase different. The computation for this case is carried out at zero drift angles. To get rid of the non-uniform disturbance, the simulation is carried out up to three periods of motion. The pressure force distribution and the shear force distribution over a period of motion are shown in Figure 11. The pressure contours on the hull surface in four quarters of period is shown in Figure 12. The vorticity distributions along the hull from the bow to the stern could be well observed in Figure 13. Each figure represents quarterly layout in one period of pure yaw movement.

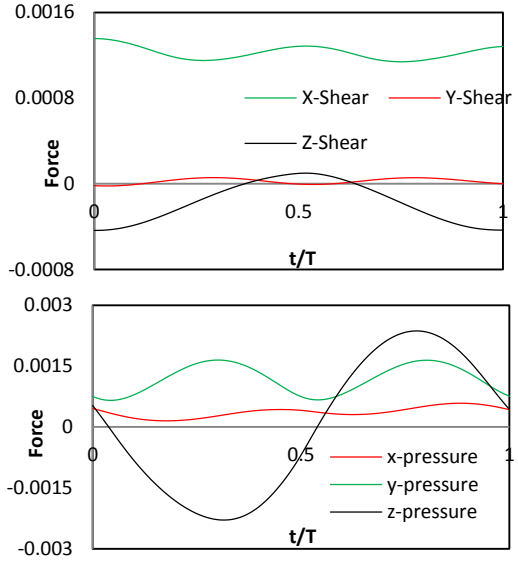

Figure 11 Shear and pressure force distributions on the hull

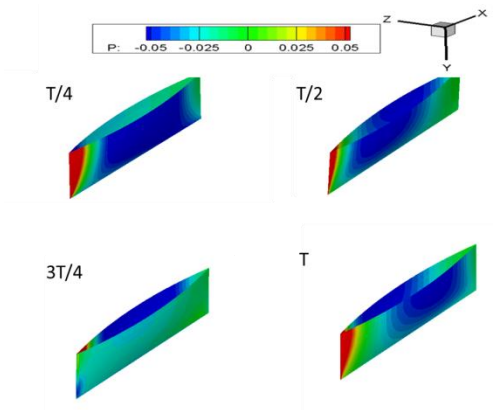

Figure 12 Pressure contours on hull surface

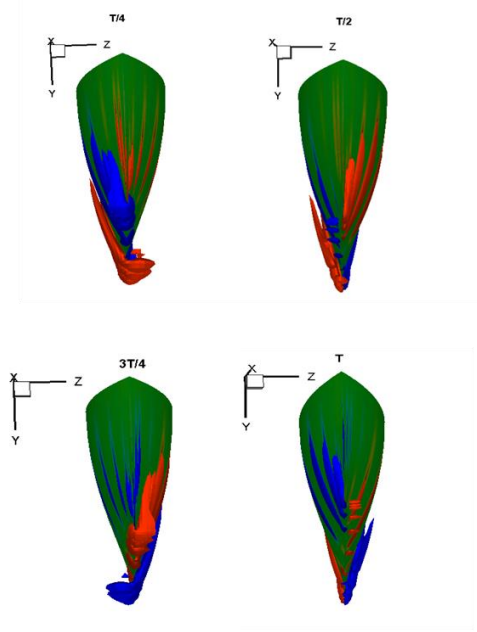

Figure 13 Vorticity distributions on the hull

3.5 Computation in Circular Motion Test

Circular Motion Test (CMT) is an important test in maneuvering field to check the ability of the rudder. This could be easily simulated in inertial frame compared to the non-inertial computation that is one of the reasons the code has been transformed. In this study, CMT is carried out for checking the hydrodynamics forces along the hull and the scope capability of the new computation code. The motion algorithm is shown in Figure 14 with the variables definitions (Equation 40-43) where the translating velocity is V_{trans}.

$$\omega = |\Omega| = \frac{d\theta(t)}{dt} = \frac{2\pi}{T} \quad (40)$$

$$V_{trans} = \Omega \times r \quad (41)$$

$$a = \Omega \times Vel \quad (42)$$

$$\theta(t) = \omega t \quad (43)$$

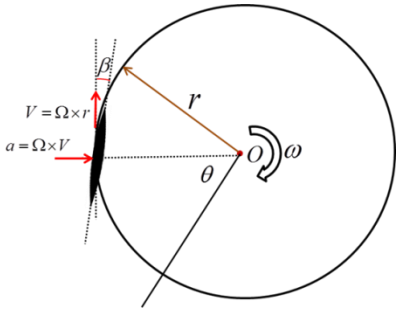

Figure 14 Motion algorithms for circular motion test

The whole domain with the ship has to move in the circular path centered at O. In this study, the center of rotation is taken reference at (0.5, 3) in (x,z) plane with the turning radius in inertial frame. The rate of rotation or frequency ω (Equation 40) is kept at constant at 0.2. In order to achieve the circular motion with the centripetal force towards the center O, some drift angle β is imposed by 4 degree to the inside of the circle. The simulation is carried out for two full circles of motion and the surge force (x-direction) and sway force (z-direction) on the ship hull in non-inertial coordinate is shown in Figure 15.

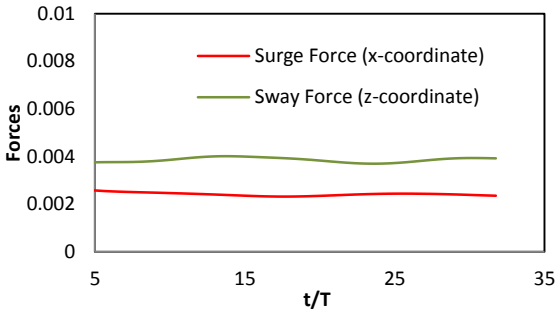

Figure 15 Hydrodynamics forces on the hull in CMT

■4.0 COMPUTATION WITH PROPELLER BODY-FORCE

The grid generated is without propeller grid inside the domain and the propeller effect is implemented by the body-force concept. The MAU five-bladed propeller which is right handed with a boss ratio of 0.2 is used. The non-dimensional propeller radius is 0.04 with a constant pitch 2.062 and is placed behind the ship at $x/L = 1.021$ centered at (0.08594, 0) on (y,z) plane. The ship is moving with $u_G = 1$ steadily and the velocity components in domain grid at propeller section are transferred into the polar coordinate of the propeller plane which had 51 grids radially with 13 sections tangentially (Figure 16) and, the number of grids is well enough to compute the body force by the blade element theory as shown in Figure 17.

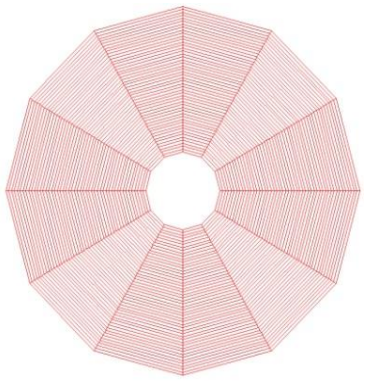

Figure 16 Grids on virtual propeller plane

$$V_R = \sqrt{u^2 + (2\pi nr - v_\theta)^2} \quad (44)$$

$$\beta_i = \arctan\left(\frac{u}{2\pi nr - v_\theta}\right) \quad (45)$$

$$C_l = 2\pi k \sin(\alpha + \alpha_{g1}) \quad (46)$$

$$k = 1.07 - 1.05\left(\frac{c_{0.7R}}{R}\right) + 0.375\left(\frac{c_{0.7R}}{R}\right)^2 \quad (47)$$

The computation procedures are as shown in Equation 44-47. When the propeller is rotating clockwise with tangential velocity v_θ, the relative velocity of the fluid anticlockwise will be $2\pi nr$ where n is the number of revolution. So the resultant velocity with induced velocity effect is computed by Equation 44 and the corresponding hydrodynamic pitch angle β_i is computed by Equation 45. The lift coefficient C_l is based on the zero lift line (dashed line in Figure 17) with k, a correction for the finite width of the propeller blade, and angle of attack $(\alpha+\alpha_{g1})$ and computed as in Equation 46 and drag coefficient C_D is assumed as 0.01.

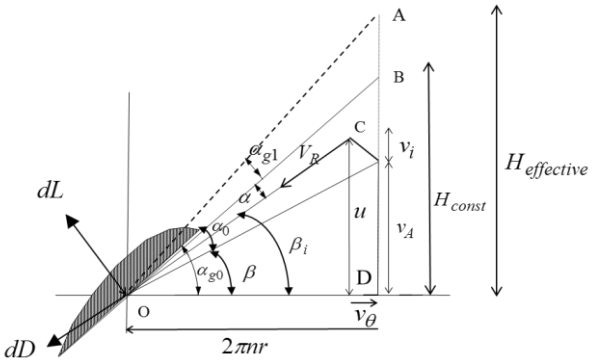

Figure 17 Concept of blade element theory

The thrust and torque forces are computed by Equation 48 and the corresponding body-forces are calculated by Equation 49 which are transmitted back into the main domain grids and implemented into the source terms of the Navier-stokes equation (Equation 24).

$$\left.\begin{aligned} dL &= 0.5 * C_l \rho V_R^2 c dr \\ dD &= 0.5 * C_D \rho V_R^2 c dr \\ dT &= dL\cos\beta_i - dD\sin\beta_i \\ dQ &= (dL\sin\beta_i + dD\cos\beta_i) * r \end{aligned}\right\} \quad (48)$$

$$\left.\begin{aligned} F_{bx} &= \frac{dT}{\Delta x}\frac{N}{2\pi\rho r dr} \\ F_{b\theta} &= \frac{dQ}{\Delta x}\frac{N}{2\pi\rho r^2 dr} \end{aligned}\right\} \quad (49)$$

In nomenclature, c is the chord length at each radius which is imported from the propeller chord length data file, dr is the radial increment, N is the number of blade, ρ is the non-dimensional density (=1) and Δx is the grid spacing respectively. The velocity distribution on the propeller plane is shown in Figure 18 and the axial velocity is seen to be higher on the right side due to the effect of right-handed propeller and flow field of the ship. The cross-flow vector on the propeller is as in Figure 19. The pressure jump on the propeller plane could be well observed in Figure 20. The propeller is given the number of rotation based on the ship advanced coefficient J_s and the result of the torque and thrust coefficient is presented in Figure 21.

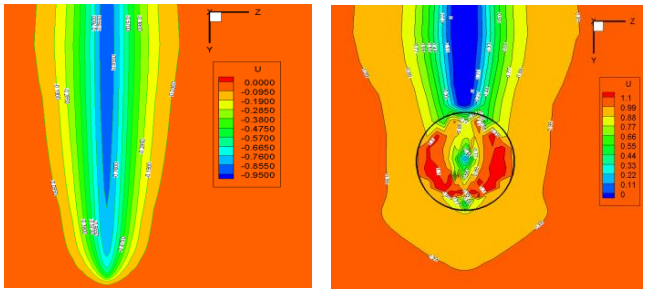

(a) Without Propeller (b) With Propeller

Figure 18 Axial velocity contours at x/L=1.021

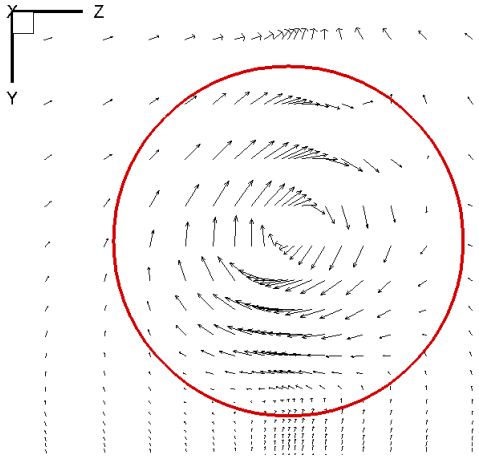

Figure 19 Cross-flow vectors on the propeller plane at x/L=1.021

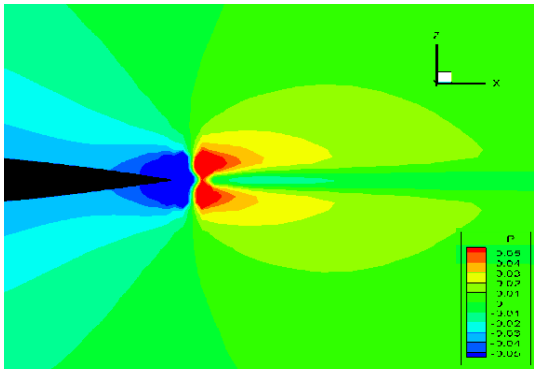

Figure 20 Pressure jump at the propeller plane

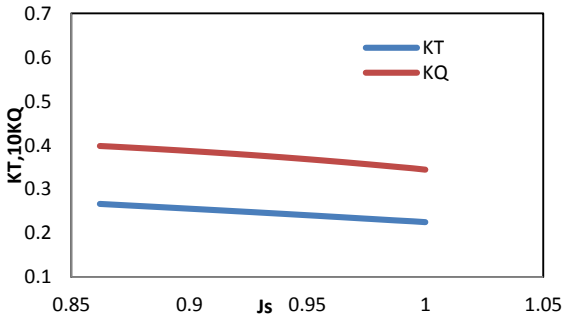

Figure 21 Thrust and torque coefficient with respect to J_s

5.0 CONCLUSION

In conclusion, the previous version of the computation code which is based on non-inertial reference frame is transformed successfully into the one in inertial frame. It is obvious that specification of boundary conditions in the new code is comparatively easier and several ship motion tests can be computed well. The new code is firstly simulated using the flat plate and the results are validated with the hydrodynamics theory as well as with the results in non-inertial frame and well agreements are observed. Using the wigley model, important maneuvering motions like pure yaw and circular motion test can be simulated well and hydrodynamics behavior around the hull is well observed. Moreover, the propeller effect by the body-force concept can be implemented behind the ship and the propulsion quantities are computed and observed well. The concept of the transformation technique, the advantage of the computation in inertial frame and the introducing of the new propeller body-force concept that are all covered in this paper is the important step which will strongly support the future research projects.

Acknowledgement

We give our special thanks to all of the members of the third laboratory, Department of Naval Architecture and Ocean Engineering, Osaka University who have involved in this research project.

References

[1] Schlichting, H. 1979. *Boundary-Layer Theory Seventh Edition*. 135: 140.
[2] Van-Dyke, M. 1982. *An Album of Fluid Motion*. 18: 22.
[3] Stern, F., Paterson, E. G., Tahara, Y. 1996. *CFDSHIP-IOWA: Computational Fluid Dynamics Method for Surfae-Ship Boundary Layers, Wakes and Wave Fields.* IIHR Report 381. 2: 33.
[4] Xing, T., Carrica, P., Stern, F. 2008. *Computational Towing Tank Procedures for Single Run Curves of Resistance and Propulsion.* 130(1): 1–4.
[5] Ueno, M., Yoshimura, Y., Tsukada, Y., Miyazaki, H. 2009. *Circular Motion Tests and Uncertainty Analysis for ship maneuverability*. 1: 3.
[6] Broglia, R., Muscari, R., Mascio, A. D. 2006. *Numerical Analysis of Blockage Effects in PMM Tests. The 26th Symposium on Naval Hydrodynamics*. 27: 28.
[7] Cura-Hochbaum, A. 2006. *Virtual PMM Test for Manoeuvring Prediction. The 26th Symposium on Naval Hydrodynamics*. 31: 40.
[8] Kuroda, K. 2012. *Graduation Thesis of Department of naval Architecture and Ocean Engineering. Osaka*. 8: 11.